

# LiDPM: Rethinking Point Diffusion for Lidar Scene Completion

Tetiana Martyniuk<sup>1,2</sup> Gilles Puy<sup>1,2</sup> Alexandre Boulch<sup>1,2</sup> Renaud Marlet<sup>1,2,3</sup> Raoul de Charette<sup>1</sup>

**Abstract**—Training diffusion models that work directly on lidar points at the scale of outdoor scenes is challenging due to the difficulty of generating fine-grained details from white noise over a broad field of view. The latest works addressing scene completion with diffusion models tackle this problem by reformulating the original DDPM as a local diffusion process. It contrasts with the common practice of operating at the level of objects, where vanilla DDPMs are currently used. In this work, we close the gap between these two lines of work. We identify approximations in the local diffusion formulation, show that they are not required to operate at the scene level, and that a vanilla DDPM with a well-chosen starting point is enough for completion. Finally, we demonstrate that our method, LiDPM, leads to better results in scene completion on SemanticKITTI. The project page is <https://astra-vision.github.io/LiDPM>.

## I. INTRODUCTION

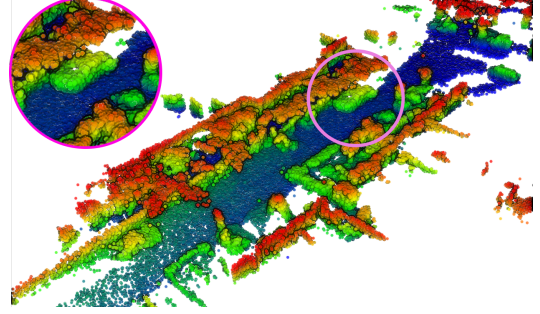
Lidars are key sensors for autonomous driving, measuring accurate distances to the vehicle environment. However, lidar point clouds are sparse, leaving wide gaps between scanned points. Yet, filling these gaps benefits downstream tasks like mapping [1], [2] or object detection [3]–[5]. Besides, acquisition patterns vary with sensor models (*e.g.*, beam count) and placement, affecting the transferability of perception algorithms (*e.g.*, detection, segmentation). There are several ways to tackle these domain gaps, such as domain adaptation [6], domain generalization [7], or scene completion [8], the latter allowing simulating new sensors by resampling the completed scene using different scan patterns. Moreover, beyond completion, generating entirely new scenes can be used to create or augment datasets.

Diffusion for point clouds offers an attractive solution for both completion and generation. In particular, direct diffusion on points, *i.e.*, moving points in 3D space without resorting to a latent scene encoding, has shown promising results [9]. One of the main advantages is that it inherently generates points, in contrast to approaches based on voxels (discretizing space) or surfaces (requiring reconstructions prior to training).

Using denoising diffusion probabilistic models (DDPMs) [10] as a basis, point diffusion has been mainly studied on small shapes (<10K pts) [11], [12], with architectures that hardly scale to large point clouds. To scale to automotive scenes (>100K pts), LiDiff [9] reformulated the problem as a local diffusion process. However, it then only allows scene completion, not generation. Besides, this local formulation introduces unnecessary approximations.

In this paper, we propose a new method, called LiDPM, that brings together these two perspectives, extending DDPMs to scenes. Our contributions are as follows:

(a) LiDPM<sup>†</sup> (ours) w/o refinement, implementing *global* diffusion



(b) LiDiff<sup>†</sup> [9] w/o refinement, implementing *local* diffusion

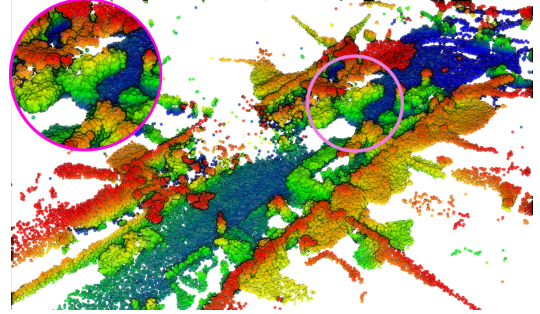


Fig. 1. **Scene-level point diffusion for completion.** Our LiDPM<sup>†</sup> formulation (top) follows the general DDPM paradigm, yielding more realistic and accurate completions than LiDiff<sup>†</sup> local diffusion [9] (bottom).

- We analyze the approximations and limitations of formulating the problem as a local diffusion.
- We show that a vanilla DDPM can be used for a global diffusion on large point clouds, thus unifying point diffusion frameworks for shapes (objects) and scenes.
- We demonstrate that LiDPM outperforms local diffusion for scene completion on SemanticKITTI [13]. Fig. 1 illustrates the quality of our results.

## II. RELATED WORK

### A. Diffusion on points

Over the past years, diffusion has been applied to various generative tasks, from image or video synthesis to speech generation. Most methods are based on DDPMs [10], which define a forward process that gradually adds Gaussian noise to the input, and a reverse process that learns to recover the input from the noise.

Methods that apply DDPMs directly to the point clouds [11], [12], [14] operate by moving points in 3D space, addressing generation or completion at the point level. In PVD [11], the conditioning for completion (concatenating sparse and noisy point cloud) imposes separate training for

<sup>1</sup> Inria, <sup>2</sup> valeo.ai, <sup>3</sup> LIGM, ENPC, Univ Gustave Eiffel, CNRS, France

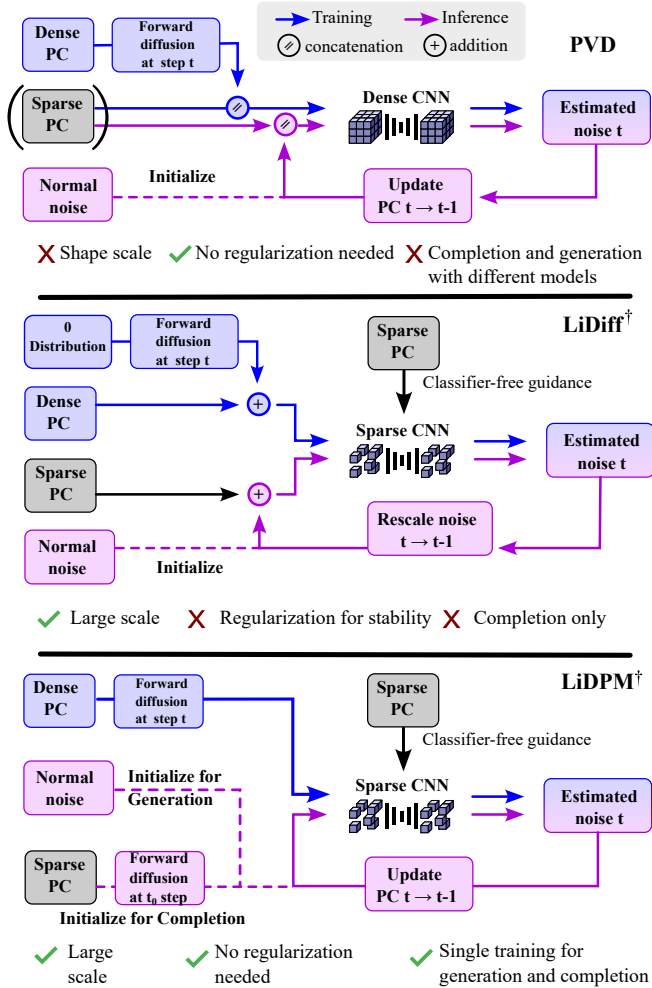


Fig. 2. **Point diffusion methods.** PVD [11] (top) applies DDPM at the object level. LiDiff [9] (middle) uses local diffusion to work at the scene level. LiDPM (bottom) makes it possible to use DDPM at the scene level.

completion and generation (Fig. 2, top). Furthermore, all the above methods focus on shapes (objects) and do not naturally scale to scene-level generation and completion.

Recently, LiDiff [9] proposed scaling the diffusion process to large scenes to complete automotive lidar scans. The authors scale up the backbone and argue for a novel “local diffusion” formulation. By doing so, LiDiff can complete scenes but at the cost of approximations, which (i) prevent using the same formulation for generation (Fig. 2, middle) and (ii) require additional regularization to stabilize training. We study these limitations in the Appendix.

In comparison, we show that we can unify the practices between the different scales (shapes/objects and scenes). Instead of a custom diffusion, we build on the original DDPM formulation (closer to the current practice for shapes), scale the backbone to allow scene completion (from a dense to a sparse CNN), and use conditioning to allow both completion and generation (Fig. 2, bottom).

### B. Scene Completion

Historically, scene completion was first achieved by completing depth or lidar data in the image space, typically

relying on custom strategies to train CNNs [15], [16]. While these methods could benefit from lightweight 2D networks, they were also inherently limited to visible areas within the field of view. Therefore, a large body of works now addresses the scene completion task in the 3D space for denser completions, also fueled by the emergence of SemanticKITTI [13], which first provided a benchmark by aggregating lidar scans. MID [2] trains a network that, given a single scan, estimates a signed distance field from voxels to the complete scene. The actual scene completion is then obtained via the Marching Cubes algorithm [17]. LODE [18] also operates at the voxel level, estimating voxel occupancy. Aside from our main objective, some methods also leverage and infer semantics [19]–[22] and are surveyed in the work of Roldão et al. [23]. However, as they operate primarily on voxels, these methods offer accuracy limited to the voxel resolution. A particular case is Local-DIFs [24], which learns an implicit function that can be queried at arbitrary positions.

**Point-based scene completion.** Closer to us, some methods operate directly on point clouds, but mainly focus on object completion [25]–[27], with few addressing large-scale point clouds like automotive lidar scans [28]. Typically, learning-based surface reconstruction algorithms train on meshes or very dense point clouds, relying on surface- or point-oriented normals. They implicitly estimate density [25] or occupancy [27] in continuous space but do not scale to scenes and still suffer from voxel-like discretization when reconstructing surfaces via the Marching Cubes algorithm. Some works tackle scene-level surface reconstruction [29], [30], but unlike our approach, they require dense input point clouds at inference, *e.g.*, aggregated scans; in contrast, we only use a single sparse lidar scan. Few methods specifically address point-based scene completion with diffusion models, such as LiDiff, as previously discussed.

## III. METHOD

LiDPM addresses the task of pointwise scene completion. It aims at predicting a dense point cloud  $\mathbf{p}^d$  from a sparse point cloud  $\mathbf{p}^s$ , typically a lidar scan. Beyond upsampling, this task is generative in that  $\mathbf{p}^s$  may suffer from large holes due to scene occlusions or sensor limitations, requiring synthesizing missing structures. To that end, we formulate the task as a denoising problem, which aims to reconstruct  $\mathbf{p}^d$  conditioned on the sparse input  $\mathbf{p}^s$ .

LiDiff [9] followed by subsequent works [31], [32] argues that the DDPM formulation [10] cannot be applied to large-scale lidar point clouds due to variations along the point cloud axes that result in a loss of details in the denoised reconstruction. Thus, they reformulate the diffusion process as *local* point denoising. Different from these works, we show that a careful formulation of the point diffusion process and relevant design choices allow an extension of DDPM to point cloud completion of large-scale urban scenes. Our diffusion process is formulated using *global* point denoising.

In this section, we first present preliminaries about DDPMs and their use for data generation (Sec. III-A). In

Sec. III-B, we detail our method, coined LiDPM, which extends DDPM to lidar point cloud completion.

#### A. Preliminaries on Diffusion Models

DDPMs [10] are generative models that iteratively transform data into Gaussian noise (forward process) and learn to reverse this process through a Markov chain of denoising steps (reverse process), possibly conditioned by another signal, such as a lidar scan for scene completion.

**The forward diffusion process** gradually corrupts a data point  $\mathbf{x}_0$ , e.g., a complete point cloud, over  $T$  discrete time steps, by adding Gaussian noise:

$$\mathbf{x}_t = \sqrt{1 - \beta_t} \mathbf{x}_{t-1} + \sqrt{\beta_t} \boldsymbol{\varepsilon}_t = \sqrt{\bar{\alpha}_t} \mathbf{x}_0 + \sqrt{1 - \bar{\alpha}_t} \boldsymbol{\varepsilon}_1, \quad (1)$$

where  $\beta_t > 0$  is a variance schedule controlling the noise level at each step  $0 < t \leq T$ ,  $\boldsymbol{\varepsilon}_t \sim \mathcal{N}(\mathbf{0}, \mathbf{I})$ , and  $\bar{\alpha}_t = \prod_{i=1}^t (1 - \beta_i)$ . For a large enough  $T$ ,  $\mathbf{x}_T$  is nearly indistinguishable from the Gaussian noise  $\mathcal{N}(\mathbf{0}, \mathbf{I})$ .

**The reverse diffusion process** seeks to sample from the original data distribution by starting from  $\mathbf{x}_T \sim \mathcal{N}(\mathbf{0}, \mathbf{I})$ . Sampling can be done iteratively applying the following formula from  $t = T$  to  $t = 1$ :

$$\mathbf{x}_{t-1} = \frac{1}{\sqrt{\alpha_t}} \left( \mathbf{x}_t - \frac{1 - \alpha_t}{\sqrt{1 - \bar{\alpha}_t}} \boldsymbol{\varepsilon}_\theta(\mathbf{x}_t, t) \right) + \sqrt{\beta_t} \mathbf{z}_t, \quad (2)$$

where  $\alpha_t = 1 - \beta_t$  and  $\mathbf{z}_t \sim \mathcal{N}(\mathbf{0}, \mathbf{I})$  if  $t > 1$  or  $\mathbf{z}_1 = \mathbf{0}$  otherwise. The network  $\boldsymbol{\varepsilon}_\theta$  in Eq. (2) is trained by minimizing

$$\begin{aligned} \mathcal{L}(\theta) &= \mathbb{E}_{\mathbf{x}_0, \boldsymbol{\varepsilon}} \|\boldsymbol{\varepsilon} - \boldsymbol{\varepsilon}_\theta(\mathbf{x}_t, t)\|^2 = \\ &= \mathbb{E}_{\mathbf{x}_0, \boldsymbol{\varepsilon}} \|\boldsymbol{\varepsilon} - \boldsymbol{\varepsilon}_\theta(\sqrt{\bar{\alpha}_t} \mathbf{x}_0 + \sqrt{1 - \bar{\alpha}_t} \boldsymbol{\varepsilon}, t)\|^2. \end{aligned} \quad (3)$$

#### B. LiDPM

Building on this diffusion process, we propose to solve scene completion by learning a diffusion model generating dense point clouds  $\mathbf{p}^d$  conditioned on sparse lidar scans  $\mathbf{p}^s$ .

Contrary to the local point denoising methods [9], [31], we show that the original diffusion process can be left intact assuming only one approximation on the starting point of the diffusion, leading to a simple and efficient formulation of scene completion.

**Diffusion on points.** In our work, the forward process satisfies Eq. (1) with  $\mathbf{x}_0 = \mathbf{p}^d$ , denoted as  $\mathbf{p}_0^d$  to emphasize the step 0. The network is trained using Eq. (3). The reverse denoising process satisfies Eq. (2) where our sole approximation is on its starting point. While it is possible to start from  $\mathbf{p}_T^d \sim \mathcal{N}(\mathbf{0}, \mathbf{I})$ , we propose to begin the diffusion process from an intermediate step  $0 < t_0 < T$ . Even though computing the starting point  $\mathbf{p}_{t_0}^d$  requires knowledge of  $\mathbf{p}_0^d$ , we show experimentally that good results are obtained by starting from

$$\tilde{\mathbf{p}}_{t_0}^d = \sqrt{\bar{\alpha}_{t_0}} \tilde{\mathbf{p}}^s + \sqrt{1 - \bar{\alpha}_{t_0}} \mathbf{z}, \quad (4)$$

where  $\tilde{\mathbf{p}}^s$  is obtained by duplicating  $K$  times the preprocessed point cloud  $\mathbf{p}^s$  (see Sec. IV, Implementation details), and  $\mathbf{z} \sim \mathcal{N}(\mathbf{0}, \mathbf{I})$ . The factor  $K$  is chosen so that the number of

points in  $\tilde{\mathbf{p}}^s$  and preprocessed  $\mathbf{p}^d$  have the same order of magnitude (typically  $K = 10$ , as in LiDiff).

**Conditioning on  $\mathbf{p}^s$ .** We use classifier-free guidance [33] to ensure that the details captured in  $\mathbf{p}^s$  are preserved in the generated point cloud. In practice, the update  $\boldsymbol{\varepsilon}_\theta(\mathbf{p}_t^d, t)$  in the reverse denoising process is replaced by

$$\tilde{\boldsymbol{\varepsilon}}_\theta(\mathbf{p}_t^d, t, \mathbf{p}^s) = (1 - \gamma) \boldsymbol{\varepsilon}_\theta(\mathbf{p}_t^d, t, \mathbf{0}) + \gamma \boldsymbol{\varepsilon}_\theta(\mathbf{p}_t^d, t, \mathbf{p}^s), \quad (5)$$

where  $\gamma > 0$  (we set  $\gamma = 6$ , as in LiDiff), and  $\boldsymbol{\varepsilon}_\theta$  is conditioned with  $\mathbf{p}^s$  or with the all-zero point cloud  $\mathbf{0}$ .

The network  $\boldsymbol{\varepsilon}_\theta$  has the architecture proposed in LiDiff, but with all batch normalization layers replaced by instance normalization. Indeed, in this architecture,  $\boldsymbol{\varepsilon}_\theta$  takes as input widely different point clouds for conditioning:  $\mathbf{p}^s$  or  $\mathbf{0}$ . We noticed that the statistics of the features may vary significantly when passing  $\mathbf{p}^s$  or  $\mathbf{0}$ , potentially corrupting the running statistics and leading to instabilities during inference. To avoid this issue, we use instance normalization layers in which the statistics of the features are computed for each instance during training and inference. We elaborate on this in Sec. IV-D.

## IV. RESULTS

**Dataset.** We train and evaluate our diffusion model on SemanticKITTI [13], preparing ground-truth point clouds as in LiDiff [9] by aggregating scans using the provided ego-poses and excluding moving objects. Training is done on sequences 00-10, with sequence 08 reserved for validation.

**Implementation details.** We train our diffusion model for 40 epochs using a batch size of 8 and Adam optimizer [34] with a constant learning rate of  $2 \cdot 10^{-4}$  and no weight decay. The diffusion parameters are linearly interpolated between  $\beta_1 = 3.5 \cdot 10^{-5}$  and  $\beta_{1000} = 0.007$ , as in LiDiff. The MinkUNet  $\boldsymbol{\varepsilon}_\theta$  [35] (adapted as in LiDiff) is trained with and without conditioning, selected randomly per iteration, with conditioning used 10% of the time. The voxel size of  $\boldsymbol{\varepsilon}_\theta$  is 5 cm. The point clouds  $\mathbf{p}^d$  and  $\mathbf{p}^s$  are cropped at a range of 50 m. The sizes of  $\mathbf{p}^s$  and  $\mathbf{p}^d$  are limited to 18K and 180K points, with farthest point sampling and uniform sampling applied to  $\mathbf{p}^s$  and  $\mathbf{p}^d$ , respectively. The generation via DPM-Solver [36] is done in 20 sampling steps. Before subsampling and  $K$ -duplicating  $\mathbf{p}^s$  to obtain  $\tilde{\mathbf{p}}^s$ , we add 1000 points uniformly sampled from a flat disc of radius 3.5 m at the ground height to compensate for points close to the car removed during the data preprocessing. Unless mentioned otherwise (with †), the diffusion output is densified with the refinement network of LiDiff used off-the-shelf.

**Metrics.** For evaluation, we follow LiDiff. We report Chamfer distance (CD), Jensen-Shannon divergence (JSD) computed in BEV and in 3D space, and occupancy IoU for different voxel sizes (0.5, 0.2 or 0.1 m).

#### A. Comparison to existing methods

**Diffusion only.** We first evaluate the quality of our learned global diffusion model, LiDPM†. We compare it to the local



TABLE I  
SEMANTICKITTI VALIDATION SET. BASELINES, METRICS AND  
GROUND-TRUTH DATA ARE FROM LiDiff [9].

Method	Output	JSD↓ 3D	JSD↓ BEV	Vox. IoU↑			CD↓
				0.5	0.2	0.1	
LMSNet [37]	Voxel	-	0.431	32.2	23.1	3.5	0.641
LODE [18]	Surface	-	0.451	43.6	47.9	6.1	1.029
MID [2]	Surface	-	0.470	45.0	41.0	17.0	0.503
PVD [11]	Points	-	0.498	21.2	8.0	1.4	1.256
LiDiff <sup>†</sup> [9]	Points	0.564	0.444	42.5	33.3	11.1	0.434
LiDPM <sup>†</sup> (ours)	Points	<b>0.532</b>	0.440	<b>45.5</b>	43.9	16.1	0.446
LiDiff [9]	Points	0.573	0.416	40.7	38.9	24.8	<b>0.376</b>
LiDPM (ours)	Points	0.542	<b>0.403</b>	44.4	<b>44.0</b>	<b>27.6</b>	0.377

<sup>†</sup>: diffusion-only, *i.e.*, without post-processing (refinement).

TABLE II  
ABLATION STUDIES.

(a) Effect of $t_0$ , starting point of the diffusion.								
Start $t_0$	Diffusion only				Diffusion + Refinement			
	CD↓	Voxel IoU↑			CD↓	Voxel IoU↑		
		0.5	0.2	0.1		0.5	0.2	0.1
1000	0.600	34.3	31.3	12.8	0.535	34.1	30.6	17.9
500	<b>0.437</b>	42.0	42.3	17.7	<b>0.370</b>	41.7	39.8	26.4
300	0.439	<b>43.2</b>	44.7	20.1	0.375	<b>43.0</b>	<b>42.4</b>	<b>30.7</b>
100	0.474	40.7	<b>45.2</b>	22.0	0.427	39.1	42.2	28.0
50	0.490	38.1	43.7	<b>22.2</b>	0.440	37.3	39.9	28.7

(b) Effect of the number of DPM-Solver [36] steps.				
Steps	CD↓	IoU 0.5	IoU 0.2	IoU 0.1
50	0.437	43.9	<b>45.1</b>	19.4
20	<b>0.428</b>	<b>44.9</b>	44.8	18.2
10	0.443	41.7	43.2	20.7
5	0.447	41.2	42.1	<b>20.9</b>

diffusion model, LiDiff<sup>†</sup>, and to PVD [11], whose results on SemanticKITTI were obtained by LiDiff authors [9]. No refinement is used after diffusion for any of these methods. The results are reported in Tab. I. We notice that LiDPM<sup>†</sup> performs better than the other diffusion-only methods on all metrics, except for the Chamfer distance (CD), where it is just 1 cm away from LiDiff<sup>†</sup>. We also remark that our method’s IoU for voxels of size 0.5 m and 0.2 m is already better than the IoU obtained by LiDiff after refinement.

**Complete method.** We then compare to all baselines, still in Tab. I. We include the refinement step used for densification in LiDiff and LiDPM. We notice that LiDPM outperforms all the others in terms of JSD BEV and IoU at 0.2 m and 0.1 m. LiDPM is also better than LiDiff in JSD 3D and IoU at 0.5 m, and reaches an equivalent CD. We only notice a slight performance drop for LiDPM before and after refinement in JSD 3D and IoU at 0.5 m. The qualitative results presented in Fig. 4 show that the generated point clouds with LiDPM exhibit less spurious structures than those generated with LiDiff, in particular far away from the center of the scenes.

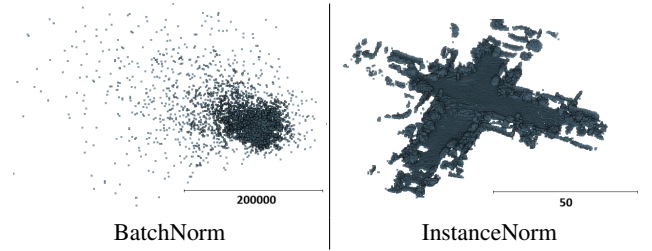


Fig. 3. **Effect of normalization.** Using batch normalization layers (left) leads to instabilities with points generated at far ranges. This is solved when using instance normalization layers instead (right). Note the scale difference.

## B. Hyperparameter study

**Reduced evaluation set.** For simplicity and faster evaluations, we conduct this study on a small subset of the validation sequence: 10 scans equally spaced in time.

**Start of the diffusion  $t_0$ .** We generate point clouds using Eq. (2) for different starting points  $t_0$ , as defined in Eq. (4), and not using the DPM-Solver. We show in Tab. II(a) that the best results are observed for  $t_0$  around 300. Starting the diffusion with  $t_0 = 50$  prevents the network from completing the point cloud (low recall), as the starting point cloud  $\tilde{\mathbf{p}}_{t_0}^d$  is not noisy enough to fill all the gaps present in  $\mathbf{p}^s$ . In contrast, picking  $t_0$  close to  $T$  improves the recall, but the original structures in  $\mathbf{p}^s$  are less preserved (lower precision). Starting at  $t_0 = 300$  is a sweet spot to optimize the Chamfer distance and the voxel IoU. The conclusion remains the same after post-processing the results with the refinement network.

**DPM-Solver.** For  $t_0 = 300$ , we study the achievable speedup to generate a point cloud by using the DPM-Solver. We test the number of steps to generate the point clouds, between 5 and 50 (see Tab. II(b)). We notice that 20 steps are enough while the results degrade when going below.

## C. Statistics of the predicted noise $\varepsilon$

In LiDiff, the authors notice that the predicted noise at the output of  $\varepsilon_\theta$  has a mean and standard deviation very far from the expected values of 0 and 1. They introduce regularization losses to enforce this behavior (see Appendix). In our method, we notice that the network  $\varepsilon_\theta$  naturally predicts the noise with zero mean. Its standard deviation is only slightly underestimated (closer to 0.6 than 1).

## D. Preventing instabilities

When training our network  $\varepsilon_\theta$  with batch normalization layers, we noticed instabilities where points were generated at very far ranges. We identified that it was due to the batch statistics, which could be quite different whether  $\varepsilon_\theta$  was conditioned or not. To avoid this issue, we replaced all batch normalization layers by instance normalization layers. The different behaviors are illustrated in Fig. 3.

## V. CONCLUSION

We have shown that vanilla DDPM can be applied to complete outdoor lidar point clouds, meaning that local point diffusion, as used in prior work [9], [31], is not necessary at the scene level. LiDPM surpasses existing point-level



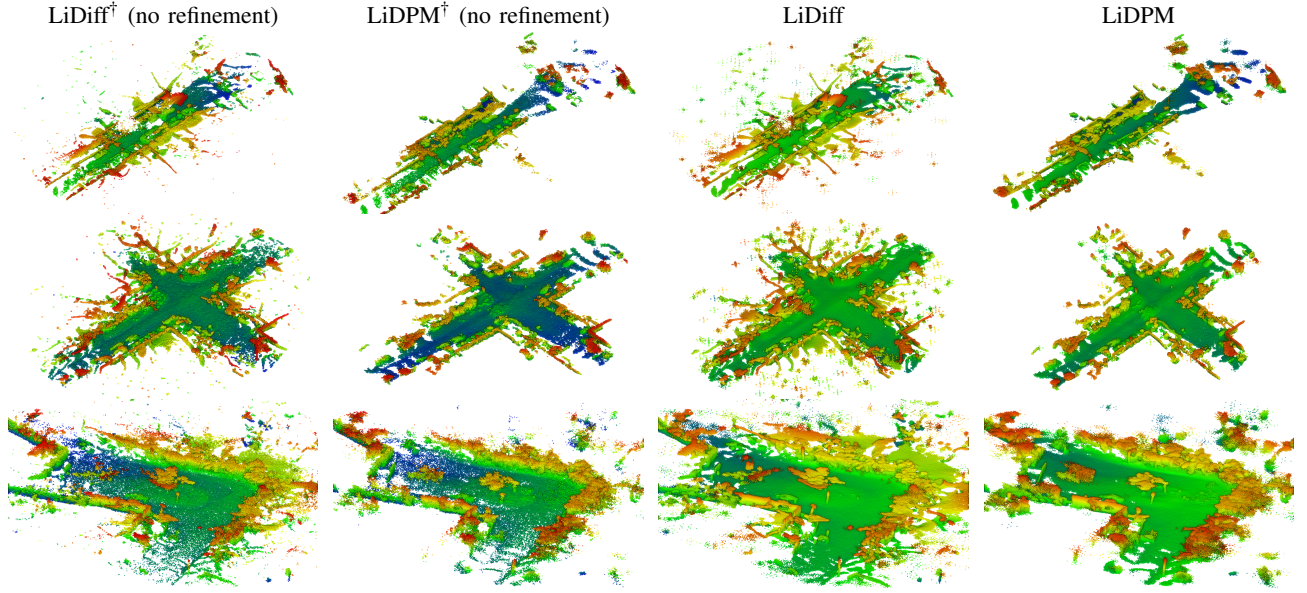


Fig. 4. **Qualitative results.** We show results from local diffusion of LiDiff w/o refinement (first column), after global diffusion at scene level with LiDPM w/o refinement (second column), with LiDiff including refinement (third column), and with LiDPM followed by refinement (last column).

diffusion-based methods on SemanticKITTI. In addition, by following DDPM formulation, LiDPM opens the door to unconditional generation, as presented in Fig. 5. This is achieved by deactivating the conditioning (setting  $\gamma = 0$  in Eq. (5)) and replacing the input scan  $\tilde{\mathbf{p}}^s$  with 180K-point clouds sampled from arbitrary shapes.

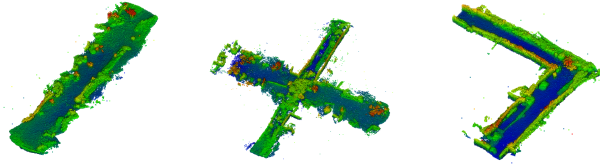


Fig. 5. **Pure generation with LiDPM.** We generate scenes unconditionally, from arbitrary point clouds following a straight, crossing, or turn shape.

## APPENDIX

We present here the formulation of the diffusion process as a *local* denoising, as discussed and used in prior work [9], [31]. We then highlight our concerns, arguing that this approach can be more complex and may introduce approximations in the denoising process.

### A. Formulation of the diffusion process as a local denoising

Starting from a dense point cloud  $\mathbf{p}_0^d$ , the forward process in LiDiff [9] satisfies

$$\mathbf{p}_t^d = \mathbf{p}_0^d + \sqrt{1 - \bar{\alpha}_t} \boldsymbol{\varepsilon}, \quad (6)$$

which is obtained by considering point offsets with respect to the ground truth  $\mathbf{p}_0^d$ , setting

$$\mathbf{x}_t = \mathbf{p}_t^d - \mathbf{p}_0^d \quad \text{and} \quad \mathbf{x}_0 = \mathbf{0} \quad (7)$$

in Eq. (1). The endpoint of this forward local diffusion process, or, equivalently, the starting point of the reverse denoising process,  $\mathbf{p}_T^d$ , is thus a noisy version of  $\mathbf{p}_0^d$ .

Second, conditioning  $\boldsymbol{\varepsilon}_\theta$  on  $\mathbf{x}_t$  as in Eq. (3) is not possible as it would require knowing  $\mathbf{p}_0^d$  during generation. Therefore,  $\boldsymbol{\varepsilon}_\theta$  is instead conditioned on  $\mathbf{p}_t^d$  and trained to minimize

$$\mathcal{L}(\theta) = \mathbb{E}_{\mathbf{p}_t^d} \left[ \|\boldsymbol{\varepsilon} - \boldsymbol{\varepsilon}_\theta(\mathbf{p}_t^d, t)\|^2 + \lambda \mathcal{L}_{\text{reg}}(\boldsymbol{\varepsilon}_\theta(\mathbf{p}_t^d, t)) \right], \quad (8)$$

$$\text{with } \mathcal{L}_{\text{reg}}(\boldsymbol{\varepsilon}_\theta(\mathbf{p}_t^d, t)) = \mathcal{L}_{\text{mean}}(\boldsymbol{\varepsilon}_\theta(\mathbf{p}_t^d, t)) + \mathcal{L}_{\text{std}}(\boldsymbol{\varepsilon}_\theta(\mathbf{p}_t^d, t)),$$

where  $\lambda > 0$ , and  $\mathcal{L}_{\text{mean}}, \mathcal{L}_{\text{std}}$  return the mean and standard deviation of the entries in  $\boldsymbol{\varepsilon}_\theta(\mathbf{p}_t^d, t)$ . When setting  $\lambda = 0$ , the LiDiff authors noticed that the mean and standard deviation of  $\boldsymbol{\varepsilon}_\theta$  were far from 0 and 1, while  $\boldsymbol{\varepsilon} \sim \mathcal{N}(\mathbf{0}, \mathbf{I})$ . Thus, the regularization loss  $\mathcal{L}_{\text{reg}}$  was introduced to guide the outputs of  $\boldsymbol{\varepsilon}_\theta$  towards these expected values.

Third, using Eqs. (7) in (2), the reverse denoising becomes

$$\mathbf{p}_{t-1}^d = \mathbf{p}_0^d + \frac{\mathbf{p}_t^d - \mathbf{p}_0^d}{\sqrt{\alpha_t}} - \frac{(1 - \alpha_t) \boldsymbol{\varepsilon}_\theta(\mathbf{p}_t^d, t)}{\sqrt{\alpha_t(1 - \bar{\alpha}_t)}} + \sqrt{\beta_t} \mathbf{z}. \quad (9)$$

Yet, this formula is unusable in practice as it requires access to the dense ground-truth point cloud  $\mathbf{p}_0^d$ , which is unknown during generation. As a workaround, LiDiff replaces the dense point cloud  $\mathbf{p}_0^d$  by a noisy estimate  $\tilde{\mathbf{p}}^s$ , obtained by noising  $K$  duplications of the sparse point cloud  $\mathbf{p}^s$ . Ultimately, the approximate reverse denoising process writes

$$\mathbf{p}_{t-1}^d = \tilde{\mathbf{p}}^s + \frac{\mathbf{p}_t^d - \tilde{\mathbf{p}}^s}{\sqrt{\alpha_t}} - \frac{(1 - \alpha_t) \boldsymbol{\varepsilon}_\theta(\mathbf{p}_t^d, t)}{\sqrt{\alpha_t(1 - \bar{\alpha}_t)}} + \sqrt{\beta_t} \mathbf{z}. \quad (10)$$

Finally, one needs to construct a starting point  $\mathbf{p}_T^d$  of the reverse denoising process. According to the forward process in Eq. (6), a starting point can be constructed by sampling  $\mathbf{z} \sim \mathcal{N}(\mathbf{0}, \mathbf{I})$  and adding it to  $\mathbf{p}_0^d$ , i.e.,

$$\mathbf{p}_T^d = \mathbf{p}_0^d + \sqrt{1 - \bar{\alpha}_T} \mathbf{z} \simeq \mathbf{p}_0^d + \mathbf{z}, \quad (11)$$

where we use the fact that  $\sqrt{1 - \bar{\alpha}_T} \simeq 1$ , as in vanilla DDPM. Again, it would require knowing the ground truth  $\mathbf{p}_0^d$ . Instead,

the starting point is also approximated using  $\tilde{\mathbf{p}}^s$ :

$$\mathbf{p}_T^d = \tilde{\mathbf{p}}^s + \mathbf{z}, \quad \text{where} \quad \mathbf{z} \sim \mathcal{N}(\mathbf{0}, \mathbf{I}). \quad (12)$$

### B. Limitations of local denoising paradigm

While the above local point diffusion proved to work, it holds on major approximations, which we outline here.

**a.** The justification of LiDiff to propose local point diffusion is that DDPM requires normalization, which leads to compression of data along some of the point cloud axes (Sec. 3.3 of LiDiff [9]). We believe this observation may be flawed. Not only could normalization be applied within fixed bounds, but it is actually not needed for DDPM, which can be formulated in the metric space (see Sec. III-B).

**b.** A major limitation of local diffusion is the reliance on a noisy estimate  $\tilde{\mathbf{p}}^s$  of the ground truth in Eq. (9) and Eq. (12), which hinders its use for data generation, thereby losing one of the major properties of diffusion models.

**c.** Third, diffusion requires the predicted noise to converge to a zero-centered distribution. To compensate for the predicted local noise not being zero-centered, the authors add an additional regularization term  $\mathcal{L}_{\text{reg}}$  (Sec. 3.4 of LiDiff [9]), which further complexifies the optimization objective.

In this work, we show that DDPM can be applied on non-normalized point clouds without losing details after generation. Hence, the local (re-)formulation is not required (observation **a.**). Moreover, since we follow the vanilla ‘scene-level’ diffusion, our formulation does not require any additional regularization (observation **b.**). Last, a byproduct of our choices is that our simpler formulation opens up the possibility to generate point clouds (observation **c.**).

### ACKNOWLEDGMENT

This work has been carried out using HPC resources from GENCI-IDRIS (grants AD011014484R1, AD011012883R3). We thank Mickael Chen, Corentin Sautier and Mohammad Fahes for the proofreading and valuable feedback.

### REFERENCES

- [1] M. Popović, F. Thomas, S. Papatheodorou, N. Funk, T. Vidal-Calleja, and S. Leutenegger, “Volumetric occupancy mapping with probabilistic depth completion for robotic navigation,” *RA-L*, 2021.
- [2] I. Vizzo, B. Mersch, R. Marcuzzi, L. Wiesmann, J. Behley, and C. Stachniss, “Make it dense: Self-supervised geometric scan completion of sparse 3D lidar scans in large outdoor environments,” *RA-L*, 2022.
- [3] X. Wu, L. Peng, H. Yang, L. Xie, C. Huang, C. Deng, H. Liu, and D. Cai, “Sparse fuse dense: Towards high quality 3D detection with depth completion,” in *CVPR*, 2022.
- [4] Y. Xiong, W.-C. Ma, J. Wang, and R. Urtasun, “Learning compact representations for lidar completion and generation,” in *CVPR*, 2023.
- [5] Y. Shan, Y. Xia, Y. Chen, and D. Cremers, “Scp: Scene completion pre-training for 3d object detection,” in *ISPRS*, 2023.
- [6] B. Michele, A. Boulch, G. Puy, T.-H. Vu, R. Marlet, and N. Courty, “SALUDA: Surface-based automotive lidar unsupervised domain adaptation,” in *3DV*, 2024.
- [7] J. Sanchez, J.-E. Deschaud, and F. Goulette, “Domain generalization of 3D semantic segmentation in autonomous driving,” in *ICCV*, 2023.
- [8] L. Yi, B. Gong, and T. Funkhouser, “Complete & Label: A domain adaptation approach to semantic segmentation of lidar point clouds,” in *CVPR*, 2021.
- [9] L. Nunes, R. Marcuzzi, B. Mersch, J. Behley, and C. Stachniss, “Scaling diffusion models to real-world 3d lidar scene completion,” in *CVPR*, 2024.
- [10] J. Ho, A. Jain, and P. Abbeel, “Denoising diffusion probabilistic models,” in *NeurIPS*, 2020.
- [11] L. Zhou, Y. Du, and J. Wu, “3d shape generation and completion through point-voxel diffusion,” in *ICCV*, 2021.
- [12] S. Mo, E. Xie, R. Chu, L. Hong, M. Niessner, and Z. Li, “Dit-3d: Exploring plain diffusion transformers for 3d shape generation,” in *NeurIPS*, 2023.
- [13] J. Behley, M. Garbade, A. Milioto, J. Quenzel, S. Behnke, C. Stachniss, and J. Gall, “Semantickitti: A dataset for semantic scene understanding of lidar sequences,” in *CVPR*, 2019.
- [14] S. Luo and W. Hu, “Diffusion probabilistic models for 3d point cloud generation,” in *CVPR*, 2021.
- [15] F. Ma and S. Karaman, “Sparse-to-dense: Depth prediction from sparse depth samples and a single image,” in *ICRA*, 2018.
- [16] M. Jaritz, R. De Charette, E. Wirbel, X. Perrotton, and F. Nashashibi, “Sparse and dense data with cnns: Depth completion and semantic segmentation,” in *3DV*, 2018.
- [17] W. E. Lorensen and H. E. Cline, “Marching cubes: A high resolution 3D surface construction algorithm,” in *SIGGRAPH*, 1987.
- [18] P. Li, R. Zhao, Y. Shi, H. Zhao, J. Yuan, G. Zhou, and Y.-Q. Zhang, “LODE: Locally conditioned eikonal implicit scene completion from sparse lidar,” in *ICRA*, 2023.
- [19] L. Roldão, R. de Charette, and A. Verroust-Blondet, “LMSCNet: Lightweight multiscale 3D semantic completion,” in *3DV*, 2020.
- [20] Z. Xia, Y. Liu, X. Li, X. Zhu, Y. Ma, Y. Li, Y. Hou, and Y. Qiao, “Scpnet: Semantic scene completion on point cloud,” in *CVPR*, 2023.
- [21] S. Song, F. Yu, A. Zeng, A. X. Chang, M. Savva, and T. Funkhouser, “Semantic scene completion from a single depth image,” in *CVPR*, 2017.
- [22] X. Yan, J. Gao, J. Li, R. Zhang, Z. Li, R. Huang, and S. Cui, “Sparse single sweep lidar point cloud segmentation via learning contextual shape priors from scene completion,” in *AAAI*, 2021.
- [23] L. Roldão, R. De Charette, and A. Verroust-Blondet, “3d semantic scene completion: A survey,” *IJCV*, 2022.
- [24] C. B. Rist, D. Emmerichs, M. Enzweiler, and D. M. Gavrila, “Semantic scene completion using local deep implicit functions on lidar data,” *T-PAMI*, 2022.
- [25] R. Cai, G. Yang, H. Averbuch-Elor, Z. Hao, S. Belongie, N. Snavely, and B. Hariharan, “Learning gradient fields for shape generation,” in *ECCV*, 2020.
- [26] W. Yuan, T. Khot, D. Held, C. Mertz, and M. Hebert, “Pcn: Point completion network,” in *3DV*, 2018.
- [27] A. Boulch, P.-A. Langlois, G. Puy, and R. Marlet, “NeeDrop: Self-supervised shape representation from sparse point clouds using needle dropping,” in *3DV*, 2021.
- [28] R. Sulzer, L. Landrieu, A. Boulch, R. Marlet, and B. Vallet, “Deep surface reconstruction from point clouds with visibility information,” in *ICPR*, 2022.
- [29] I. Vizzo, X. Chen, N. Chebrolu, J. Behley, and C. Stachniss, “Poisson surface reconstruction for lidar odometry and mapping,” in *ICRA*, 2021.
- [30] J. Huang, Z. Gojic, M. Atzmon, O. Litany, S. Fidler, and F. Williams, “Neural kernel surface reconstruction,” in *CVPR*, 2023.
- [31] S. Zhang, A. Zhao, L. Yang, Z. Li, C. Meng, H. Xu, T. Chen, A. Wei, P. P. GU, and L. Sun, “Distilling diffusion models to efficient 3d lidar scene completion,” *arXiv:2412.03515*, 2024.
- [32] H. Cao and S. Behnke, “DiffSSC: Semantic lidar scan completion using denoising diffusion probabilistic models,” *arXiv:2409.18092*, 2024.
- [33] J. Ho and T. Salimans, “Classifier-free diffusion guidance,” in *NeurIPS Workshop*, 2021.
- [34] D. P. Kingma and J. Ba, “Adam: A method for stochastic optimization,” in *ICLR*, 2015.
- [35] C. Choy, J. Gwak, and S. Savarese, “4D spatio-temporal ConvNets: Minkowski convolutional neural networks,” in *CVPR*, 2019.
- [36] C. Lu, Y. Zhou, F. Bao, J. Chen, C. Li, and J. Zhu, “DPM-Solver: A fast ODE solver for diffusion probabilistic model sampling in around 10 steps,” in *NeurIPS*, 2022.
- [37] L. Roldão, R. de Charette, and A. Verroust-Blondet, “Lmscnet: Lightweight multiscale 3d semantic completion,” in *3DV*, 2020.